Reproducible Patterning of Single Au Nanoparticles on Silicon Substrates by Scanning Probe Oxidation and Self-Assembly

Xing Ling, Xin Zhu, Jin Zhang,* Tao Zhu, Manhong Liu, Lianming Tong, and Zhongfan Liu*

College of Chemistry and Molecular Engineering, Center for Nanoscale Science and Technology (CNST), Peking University, Beijing 100871, China

Received: September 28, 2004; In Final Form: November 16, 2004

This paper describes a rational approach for reproducibly patterning single Au nanoparticles, 15−20-nm diameter, on silicon wafer substrates. The approach uses scanning probe oxidation (SPO) to pattern silicon oxide nanodomain arrays on silicon substrates modified with octadecyltrimethoxysilane (OTS). It was usually found using aminopropyltrimethoxysilane (APS) that Au nanoparticles only assembled at the domain boundaries probably because of asymmetrically distributed hydroxyl groups. To generate uniformly distributed hydroxyl groups on oxide domains, we employed a two-step treatment to etch and oxidize the substrate. With this treatment, oxide domains consistently attached Au nanoparticles to maximum capacity. Single Au nanoparticles were readily patterned by fabricating oxide nanodomains with a diameter below 30 nm. We also investigated the deposition of APS on OTS monolayers, which resulted in the assembly of Au nanoparticles outside of the oxide domains, and proposed two alternative methods to inhibit it.

Introduction

Precise position of nano-objects produced by various chemical routines is critically required for ultimate nanostructuring. The mainstream methodologies for this involve direct manipulation of the nano-objects by atomic force microscope (AFM)[1] or guided self-assembly on a well-defined template via capillary interaction,[2] electrostatic attraction,[3,4] or covalent bonding.[5] Compared with low-throughput AFM manipulation, flexible and high-throughput self-assembly strategies are more amenable to large-scale nanostructuring. Employing nanometer-resolution lithography, sub-100-nm nano-objects were precisely positioned.[6,7] Particularly, using SPO, which directly oxidizes a substrate by applying an intensive electrical field at tip−sample junction, a template of patterned oxide domains, 28-nm diameter, was fabricated on a silicon substrate. Deriving the oxide domains with APS led to precise position of single 15-nm Au nanoparticles that were perfectly guided by the template.[3] This strategy does not apply any principle limitation to the choice of other organosilanes possessing specific affinities for various colloids; in general, any nano-object that could self-assemble on silicon surfaces has the chance to be patterned by the combination of SPO and self-assembly involving versatile layer-by-layer assembly. The patterned nano-objects could find many potential applications in biology, electronics, optics, and controlled growth of nanostructured materials.[8]

However, because of lack of understanding of chemical properties of silicon oxide produced by SPO, the chemical derivation of the oxide could not be conducted in an efficient way. For example, the bonding of single Au nanoparticles to single oxide domains was found only on 30% of the domains.[3] To make this strategy reliable for patterning single nano-objects such as 15-nm Au nanoparticles, the surface properties of oxide produced by SPO need to be further explored. In this work, using Au nanoparticles for APS labeling, we investigated the adsorption of APS on the oxide nanodomains, which were produced on OTS monolayer-covered silicon substrates by ambient SPO. APS located preferentially at the boundaries of oxide domains. This phenomenon appeared to result from the asymmetric distribution of hydroxyl groups on the oxide domains, since after the hydroxyl regeneration of oxide by etching the substrate in ammonium fluoride followed by oxidation in peroxide, Au particles were not limited to the domain edge but homogeneously covered the entire oxidized domain. The hydroxyl regeneration was the same efficiency for oxide domains of different sizes. This guaranteed the controlling of particle number solely by tuning the size of oxide domains and made the bonding of single Au nanoparticles to single domains of size below 30 nm reproducible.

We also investigated the deposition of APS outside oxide domains, which appeared to be closely related to reactive groups and surface water on the OTS monolayers. With heating or exchanging of anhydrous solvent to reduce surface water physisorbed on the OTS monolayers, such an unwanted deposition of APS and Au nanoparticles was avoided on samples with closely packed OTS monolayers. Wiping samples with cotton swabs and reimmersion in suspensions of Au nanoparticles selectively removed APS and Au nanoparticles deposited outside oxide domains.

Experimental Section

1. Materials. Octadecyltrimethoxysilane ($(CH_3O)_3Si(CH_2)_{17}CH_3$, OTS, 95%), aminopropyltrimethoxysilane ($(CH_3O)_3Si(CH_2)_3NH_2$, APS, 97%), and $HAuCl_4 \cdot 3H_2O$ (>98%) were purchased from Aldrich. The other reagents were of analytical grade and were used as received. Water of Milli-Q quality was used throughout the experiments.

2. Preparation of Au Nanoparticles. Au nanoparticles of diameter 15−20 nm were synthesized according to Frens' method.[9]

3. Preparation of OTS SAMs. Substrates cut from p-type Si (111) wafers, with a resistivity of 8−12 Ωcm, were cleaned

* To whom correspondence should be addressed. E-mail: jinzhang@pku.edu.cn. Telephone and fax: (86)-10-6275-7157.

10.1021/jp0456077 CCC: $30.25
Published on Web 01/20/2005

in 90 °C Piranha solution (H_2SO_4/H_2O_2 = 7:3, v/v), copiously rinsed with water, and blown dry with high purity nitrogen. An OTS monolayer was deposited on these substrates by chemical vapor deposition (CVD)[10] as follows. Cleaned substrates and a weighing bottle (Φ2 cm × 2 cm) filled with 100 μL OTS were placed together in a 78 cm^3 (Φ3 cm × 11 cm) cylindrical Teflon container. The container was then sealed and placed in an oven set at 150 °C. Two-hours later, the container was taken out of the oven and allowed to cool to room temperature. The samples with OTS monolayers were removed from the Teflon container and stored in a desiccator. The contact angle of the sample with water was measured on OCA 20 (Dataphysics) using sessile drop method with 5-μL droplets.

4. Scanning Probe Oxidation (SPO). Before SPO, the silicon substrate with OTS monolayer was sonicated in toluene for 10 min and then baked at 100 °C for 2 h. To perform SPO either in contact or in tapping mode, a Multimode Nanoscope III SPM (Veeco) with a HP 8114A programmable pulse generator, working as the voltage source, was used. In contact mode, the cantilever A of NSC11 (MikroMasch) was used (force constant k = 3.0 Nm^{-1}). In tapping mode, cantilever B was used (force constant k = 48 Nm^{-1}).

With feedback switched on, the probe was programmed to move to a patterned series of predefined positions. In contact mode, the same setpoint as used for imaging was employed, while in tapping mode the setpoint was reduced to 0.2−0.3 V with free amplitude of 2−3 V. On reaching each predefined position, the probe stopped and, to degrade the OTS monolayer at this position and oxidize underlying silicon substrate, a voltage pulse was applied between the tip and the monolayer-covered substrate. The probe then moved to the next predefined position. In tapping mode, the feedback was turned off before the pulse and was resumed after it to maintain the constant tip−substrate distance. This process was repeated until an entire pattern of oxidized nanodomains was obtained. The diameter of oxidized domains depended on the probe, sample, ambient humidity, and voltage and duration of pulse (6−18 V, 10−500 ms).

5. Regeneration of Hydroxyl Groups on Oxidized Domains. After SPO, the sample was etched in NH_4F/H_2O (2%, wt/v) for 3 min and immersed in acidic peroxide solution (36% HCl/30% H_2O_2/H_2O = 1/6/36, v/v/v) for 10 min. The HCl was added to H_2O_2 to enhance the oxidation of Si−H bonds formed after ammonium fluoride etching. After copious rinsing with water, the sample was blown dry with high purity N_2.

6. Assembly of APS Monolayer and Au Nanoparticle Labeling. Before assembly of APS monolayer, the sample was pretreated by one of two alternative procedures for dehydration outside of the oxide domains. The first procedure was heating the sample at 60 °C for 10 h. The second procedure is similar to that described by Zhang et al.,[11] which comprised successive rinsing with methanol, a 1:1 mixture of methanol and toluene, and sonication in toluene for 10 min. After either of these two pretreatments, the sample was immersed in APS/toluene solution (0.02%, v/v) for 30 min. A posttreatment, to remove APS adsorbed outside oxidized domains, was achieved by successive rinsing with toluene, immersion in toluene for 30 min, sonication in toluene for 10 min, and an additional rinsing with toluene, a 1:1 mixture of methanol and toluene, and methanol. The sample was baked at 100 °C for 30 min to promote the formation of siloxane bonds between APS and substrate. After copious rinsing with methanol and water, the sample was immersed in a suspension of Au nanoparticles for 20 min, followed by a final rinsing with water.

7. Wiping and Readsorption Cycle. On some samples, possibly because of contamination of the substrate or poor quality of the OTS monolayer, a very high density of gold particles was observed outside of the oxidized domain pattern. This could be removed by mechanical wiping with cotton swabs and reimmersion in colloidal Au. Repetition of this procedure produced very good removal of Au particles outside of the nanodomain pattern.

Results and Discussion

Au nanoparticles, formed by the reduction of $AuCl_4^-$ with trisodium citrate, are negatively charged because of the adsorption of anions such as citrate, chloride, Au chloride ($AuCl_4^-$), and hydroxide.[12] When APS monolayers were immersed into the suspension of Au nanoparticles, their top amino groups were protonated since the pK_a (7.5)[13] of amino groups of APS monolayers is smaller than the pH (∼6.5) of the suspension. Therefore, negatively charged Au nanoparticles can be assembled on APS monolayers with positively charged amino groups by electrostatic interaction.[14] Using this concept, a binary pattern can be generated with two groups with different affinities for Au nanoparticles. For example, a pattern composed of amino and methyl groups would restrict assembly of Au nanoparticles to predetermined domains of positively charged amino groups.[3,4,15] It would even be possible to position single Au nanoparticles by employing SPO to produce a pattern of domains each of a size comparable to a single Au nanoparticle. However, without careful control of surface properties of oxide domains, low-quality APS films were usually prepared on these domains, which reduced the reproducibility of positioning Au nanoparticles. Particularly, for oxide domain diameters of ∼70 nm, only 70% of 16 domains had attracted single Au nanoparticles; when the diameter was reduced to 28 nm, the situation was even worse with only 30% of 25 domains having single Au nanoparticles attached to them.[3] High-quality APS films on oxide domains, on the other hand, are expected to have Au nanoparticles, with an interparticle distance nearly double that of the particle diameter, homogeneously distributed on the entire surface of these domains.[16] Therefore, for an oxide domain diameter of ∼70 nm, at least two or three 15-nm-diameter Au nanoparticles (in triangular conformation) would be on top of it; for a 28 nm-diameter domain, it would always have one Au nanoparticle. With only such a saturated coverage of Au nanoparticles realized on oxide domains of different sizes, the precise control of particle number on domains by modulating the domain size could be reproducibly applied.

To achieve this goal, we modified existing procedures for domain patterning, as illustrated in Scheme 1. A closely packed OTS monolayer was prepared on a silicon substrate by CVD. SPO was then performed on the OTS monolayer in contact or tapping mode. For simplicity, humidity was not controlled and was usually in the range 20−40% during the experiments. The oxide domains produced by SPO were etched by ammonium fluoride and were oxidized using acidic peroxide before modification with APS. With appropriate pretreatment to dehydrate the sample surfaces outside of oxide domains, samples were then immersed in a solution of APS and subsequently in a suspension of Au nanoparticles to assemble Au nanoparticles on the patterned template.

Before entering the discussion of the hydroxyl-regeneration effect, we would like to first address the possible reason responsible for the low-quality APS films on oxide domains without etching and oxidation. The number of particles adsorbed on oxide domains of comparable size varied with experiments.

SCHEME 1: Diagram Showing on a Methyl-Terminated Silicon Substrate the Fabricating Process of a Template Homogeneously Covered with Hydroxyl Groups and Selective Self-Assembly of APS and Au Nanoparticles to the Template

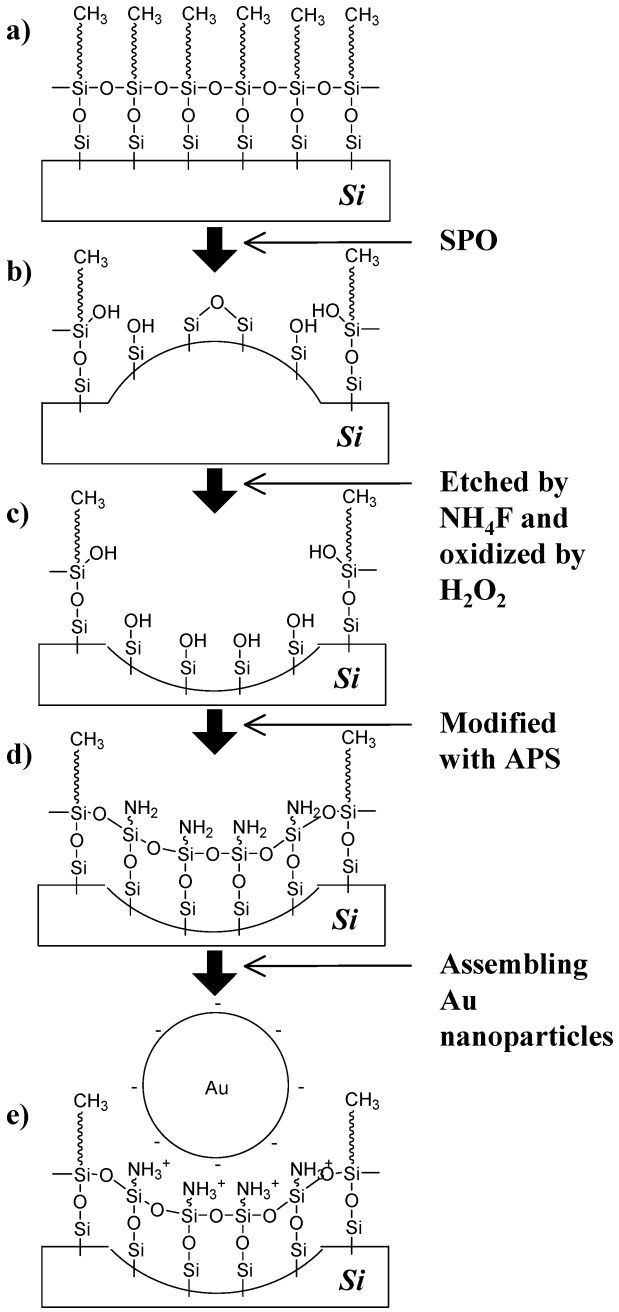

Typically, the particle adsorption state was like the one shown in Figure 1a. On this sample, while oxide domains of small diameter yielded an inefficient assembly of Au nanoparticles as described before,[3] an interesting phenomenon was simultaneously observed with oxide domains of relatively large diameter. Au nanoparticles appeared to locate primarily at the domain boundaries. (It is difficult to detect the position of particles on oxide domains in which size is smaller than the apparent width of >40 nm of 15-nm Au nanoparticles). On the other hand, very rarely (only on two samples out of dozens of samples prepared under similar conditions in different experiments) was a more integrated structure found with the domain surfaces entirely covered with particles (Figure 1b). Since for all of these experiments the same posttreatment was employed,

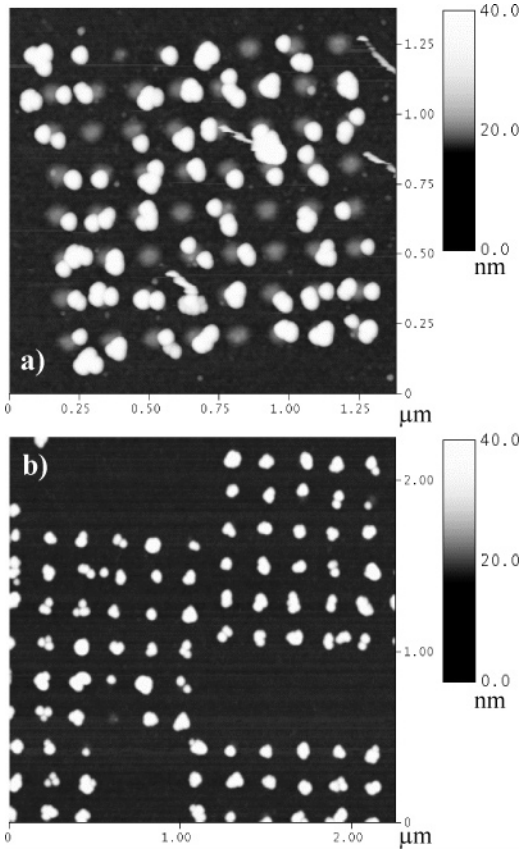

Figure 1. Tapping mode AFM topographic images indicating adsorption states of APS labeled with Au nanoparticles on different oxide domains. (a) Usually observed (the oxide formed with tapping SPO using 11 V pulse voltage, 500 ms duration, and 0.3 V setpoint and had an average height of 3.1 nm and width of 130 nm). (b) Very rarely observed (the oxide formed with tapping SPO using 12 V, 80−200 ms, and 0.3 V and had an average height of 2.3−2.7 nm and width of 74−87 nm). The height and width were measured from height images of oxide domains not shown here.

this situation almost certainly must arise from differences in the surface properties of the oxide domains. The formation of silicon oxide by SPO relates to various parameters, such as the amplitude and duration of pulse, tip/substrate surface properties, tip geometry, tip−substrate distance, and humidity. Although the difficulty to quantitatively correlate the surface composition of silicon oxide with these operational parameters is obvious, we try to stress the possible role played by the water necessary for the oxidation process (Scheme 2). As the electrochemical mechanism suggested, the water-bridging tip and the sample could work as an electrochemical nanocell and could provide oxygen species for oxide growth.[17] The supply of water would influence the ratio of silicon to oxygen in oxide bodies as well as on its surfaces. Since surface water on hydrophobic OTS monolayer prepared under anhydrous conditions can be neglected, the bridging water would be mainly supplied from the atmosphere by field-enhanced capillary condensation.[18] For a conical tip aligned perpendicular to a sample, the extremely narrow gap between tip end and sample would hinder water uptake. However, growth rate of oxide would be fastest at this site corresponding to the strongest electrical field and would require relatively large amounts of OH^- and O^{2-} ions generated by electrolysis of water. An inefficient water supply could favor the formation of Si−O−Si bonds on the oxide domain centers, since these bonds have a lower ratio of oxygen to silicon than Si−OH bonds. Away from the tip end, the oxidation of domain boundaries would take place in a relatively weak electrical field

SCHEME 2: Formation Mechanism of Asymmetrically Distributed Hydroxyl Groups on Oxide Domains during SPO[a]

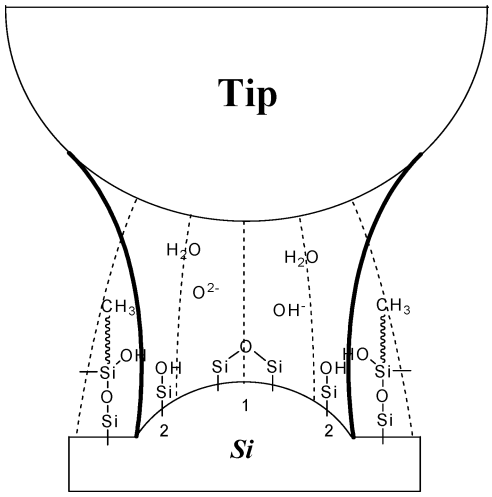

[a] (1) Domain centers composed of Si−O−Si bonds. (2) Domain boundaries composed of Si−OH bonds. Dashed lines indicate the distribution of electrical field beneath tip. Bold lines indicate the water bridging between tip and sample that was condensed from atmosphere.

and more capacious and open environments, which could facilitate the water supply and promote the formation of Si−OH bonds. Since the bonding of APS to substrates requires hydroxyl groups,[19] the asymmetric distribution of hydroxyl groups on oxide domains would confine the assembly of APS and Au nanoparticles to the domain boundaries, as indicated in Figure 1a. This hypothesis that inefficient water supply could inhibit the formation of hydroxyl groups on oxide surfaces is supported by the work of Inoue et al.,[20] who applied field-induced oxidation (FIO) at a humidity of less than 1%. Under this condition, they produced oxide layers that were inactive to octadecyltrichlorosilane (OTCS). Otherwise, when the FIO was applied at a humidity of 88%, they produced oxide layers that similarly reacted with OTCS as native oxide. Besides using SPO at a very high humidity, water supply could also be enhanced by increasing tip−sample distance under certain circumstance. For example, Garcia et al.[18] performed noncontact SPO, where the tip vibrated a few nanometers above the sample, and observed after SPO the damping of tip oscillation amplitude because of water-induced capillary attraction between tip and sample. Tapping SPO could similarly enhance water supply to produce uniformly distributed hydroxyl groups on oxide domains, which possibly explained why the complete coverage of Au nanoparticles on oxide domains could be obtained (Figure 1b).

Concluded from the above analysis, to facilitate complete coverage of oxide domains with Au nanoparticles, a homogeneous coverage of silanol on these domains was necessary. To obtain rich content of hydroxyl groups on oxide, instead of separately manipulating the operation parameters for each probe, oxide domains produced under different conditions were simply subjected to etching and oxidation in two stages. This two-step treatment generated uniformly distributed hydroxyl groups on those domains, which led to complete coverage of Au nanoparticles on the domain surfaces as shown in Figure 2a. In detail, the first step was to form Si−H bonds, which could be more easily oxidized to hydroxyl groups than direct hydrolysis of Si−O−Si. To do this, the oxide was etched in NH_4F. Such etching also ensures a complete removal of any residual OTS fragments remaining after SPO. The fragments were presumed to be one of the possible reasons that prevented APS molecules from depositing on oxide domains.[3] Under the conditions described in the Experimental Section, for oxide layers that apparently protrude from the sample surface by about 1 nm (Figure 2b), etching normally produces roughly 5-nm deep pits (Figure 2c). Etched pits were easy to identify and when oxidized to form hydroxyl groups, they were completely covered with Au nanoparticles (Figure 2d). Uneven distribution of Au nanoparticles on these pits was not observed. In addition, the interparticle distance, approximately double the diameter of a gold nanoparticle, similar to that observed on saturated adsorption of Au nanoparticles on hydroxyl-terminated surfaces, suggested that silanol coverage in these pits was homogeneous. The uncovered border of pits can be clearly identified from Figure 2d even with 15-nm Au nanoparticles being very close together. Without etching, it was more difficult to define patterns since the size of oxide domains measured from AFM friction images did not agree with AFM height images. In other words, regions surrounding oxide domains that have the same apparent height as OTS monolayer could possess higher friction characteristics than the OTS monolayer. The higher friction probably reflected some disruption of the OTS monolayer or transformation of the top methyl groups of the OTS monolayer into carboxyl groups.[21] However, the high-friction regions surrounding oxide domains could sustain erosion, as evidenced by agreement between the diameter of oxide domains measured from height images and that of pits (Supporting Information I).

The enhanced efficiency of bonding single Au nanoparticles to small oxide domains was demonstrated in Figure 3a. In this particular array, 28 of 36 domains (6×6), 23-nm diameter measured from a domain on which the bound particle was displaced by scanning, bound single Au nanoparticles, 4 of 36 domains bound two Au nanoparticles, and only 4 domains had no bound Au nanoparticles. Total efficiency was as high as 89%. A close examination of this sample revealed that occasional domains with no Au nanoparticles were apparently smaller than 23 nm, if not invisible, which indicated some reduction in reproducibility of SPO when its limit of resolution was approaching.

Using this technique, saturated coverage of Au nanoparticles was also easily achieved for oxide domains with different geometries, such as parallel lines (Figure 3b) or square (Figure 3c). The adsorption saturated for all domain dimensions also permits the precise control of the number of Au nanoparticles by manipulating oxide domain size.

One drawback was that while the efficiency was greatly improved by the two-step treatment, the region outside oxide domains began to attract APS and Au nanoparticles. This was considered to arise from water introduced in aqueous environments and some damage to the OTS monolayers.

Since the deposition of APS on OTS monolayers appeared to be strongly related to the quality of the OTS monolayer, CVD was employed instead of the hexadecane solvent process, which was prone to produce pinholes in the monolayer.[3] OTS monolayers produced by CVD usually had a large number of aggregates weakly attached on top of these monolayers, which could be removed by sonication in toluene to produce a flat surface suitable for the following SPO. While the contact angle of these samples with water was normally 105°, in a few cases, it dropped below 95°. One of the reasons for such a discrepancy could come from different distances between the sample and the OTS source placed at one end of the Teflon container during CVD. We measured the contact angles of different batches of samples; for each batch of samples, the contact angle dropped

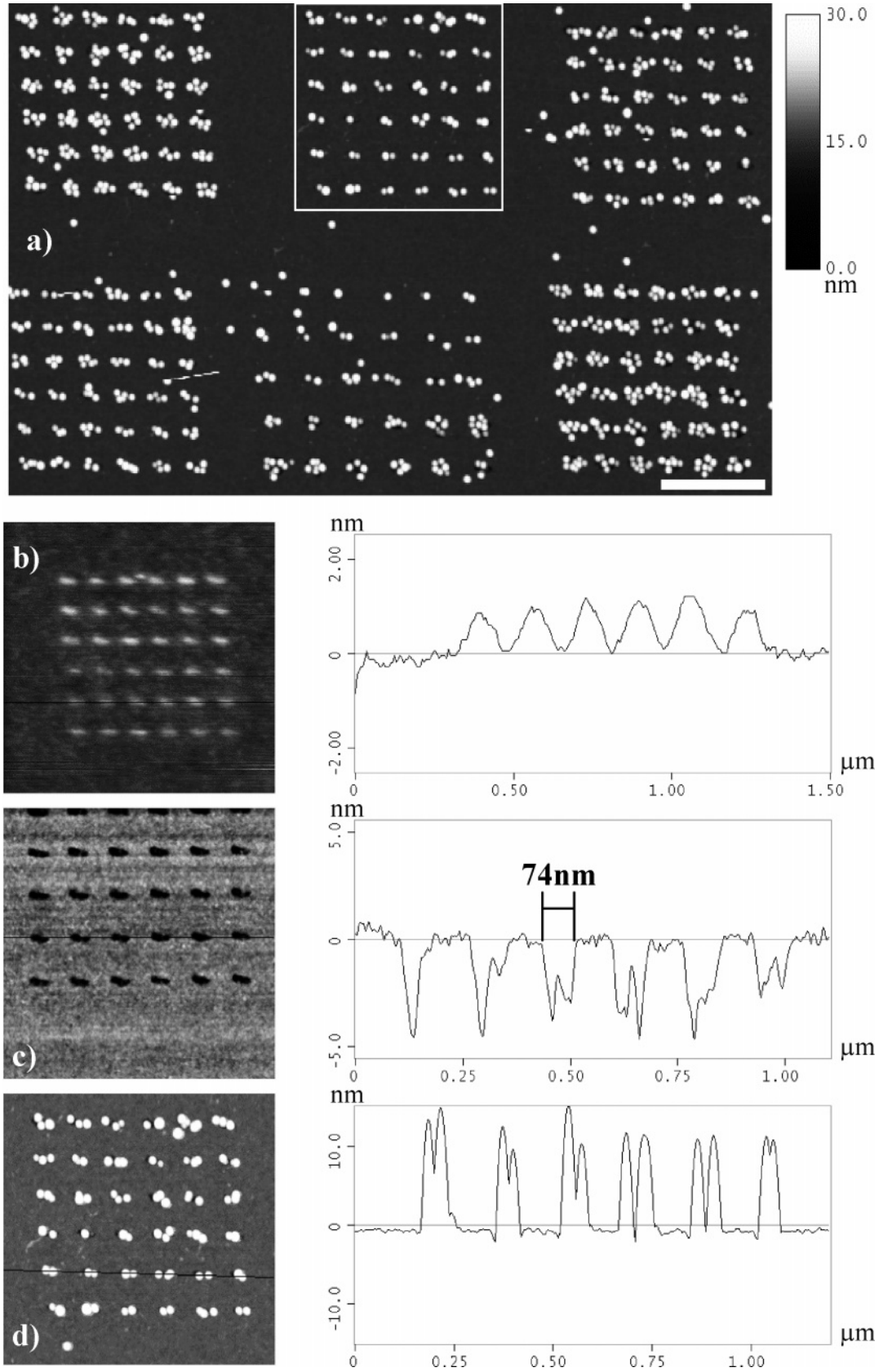

Figure 2. Tapping mode AFM topographic images of (a) as-fabricated patterns of Au nanoparticles self-assembled onto six nanodomain arrays (6 × 6) that were first etched and oxidized to generate homogeneously distributed hydroxyl groups. AFM topographic images and section analysis of (b) oxide domains in marked square, (c) pits formed by etching the oxide, and (d) saturated adsorption of Au nanoparticles on these domains using APS as linkage. Scale bar: 500 nm.

slowly with increasing the sample−OTS distance. Since the OTS vapor had to diffuse through the 2-cm-high wall of weighing bottle, which is placed perpendicularly to a cylindrical Teflon container (only 3-cm diameter), to reach the silicon substrates, a diffuse barrier could be created. Therefore, during the limited 2-h reaction time of CVD, the partial pressure of OTS possibly

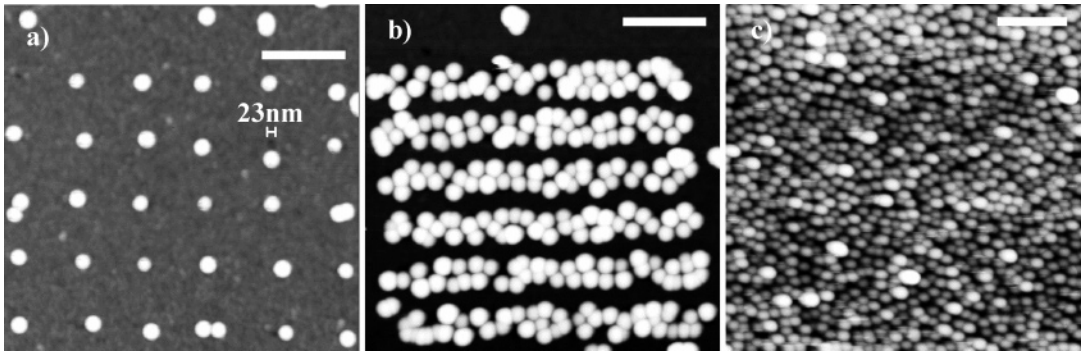

Figure 3. Tapping mode AFM topographic images of Au nanoparticles self-assembled onto etched oxide templates of different geometries: (a) an array of 36 dots with the diameter of about 23 nm, (b) six parallel lines, and (c) a square. Scale bars: (a) 200 nm, (b) 250 nm, and (c) 250 nm. Vertical range: 30 nm.

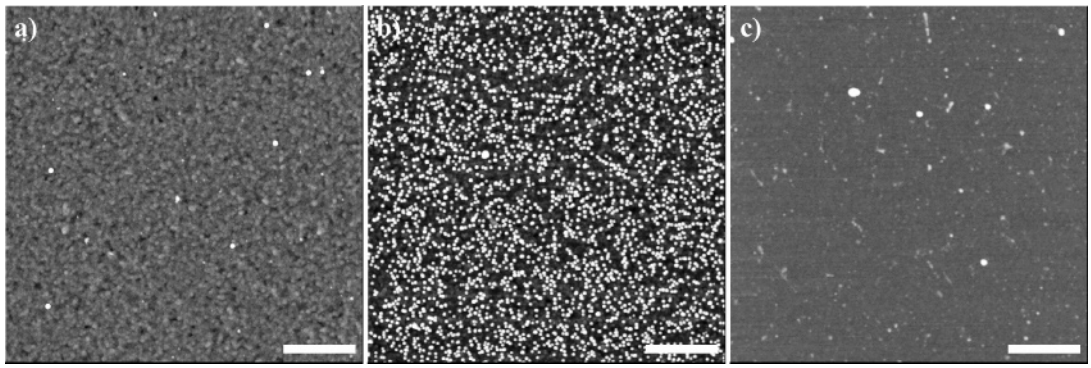

Figure 4. A Au substrate was modified sequentially with octanethiol/ethanol (1 mM, 24 h, water contact angle 105.2°), rinsed with water and ethanol, immersed in APS/ethanol (0.1%, 30 min), and finally treated with Au nanoparticles (20 min). Tapping mode AFM images show the topography of the above sample (a) before Au nanoparticles deposition, (b) after Au nanoparticles deposition. Figure 4c depicts the topography of an OTS monolayer-covered silicon substrate that was dehydrated at 120 °C and modified sequentially with APS and Au nanoparticles. Scale bars: (a, b) 1 μm, (c) 600 nm. Vertical range: 40 nm.

decreased with the sample−OTS source distance, resulting in a slower reaction rate and subsequent incomplete coverage of the OTS monolayer on substrates away from the OTS source (as far as 8 cm). These samples were unable to stop the deposition of APS and were usually discarded.

Even for an inert surface that has a physisorbed thin film of water, deposition of APS can occur. For example, a Au substrate covered with a monolayer of octanethiol has no possibility of forming chemical bonds with APS for either octanethiol-covered regions or the underlying Au substrate exposed at monolayer defects.[22] However, when such a sample was brought into contact with water first, a large amount of APS was attracted followed by Au nanoparticles, as shown in Figure 4b. The possibility that the clusters in Figure 4b could be aggregates of APS can be unambiguously excluded because before the Au nanoparticle deposition only negligible amounts of clusters existed on the surface (Figure 4a). In contrast to the large quantities of APS adsorbed on the wet surface, for a fully dehydrated OTS monolayer-covered silicon substrate, capable of forming bonds between APS and silanol at monolayer defects, the adsorption of APS was completely inhibited as indicated in Figure 4c.

A possible mechanism for water-mediated deposition of APS on inert surfaces, such as the above methyl-terminated monolayers, is as follows. First, APS rapidly binds top layers of surface water through hydrogen bonds, such as $-H_2N\cdots HOH$ or $-Si-OH\cdots HOH$. This is followed by further hydrolysis of APS by underlying surface water and condensation to form polymeric siloxane.[23] Because of the increased van de Waals attraction between the methyl-terminated surface and polymeric APS, their removal becomes difficult. For the Au substrate modified sequentially with octanethiol, APS, and Au nanoparticles, no obvious detachment of Au nanoparticles was observed even after sonication in ethanol for 10 min. This was only achieved by sonication in water for ∼13 min probably because of hydrolysis and dissolution of polymeric APS during sonication. Removal of APS adsorbed on methyl-terminated surface by sonication in water, however, damaged adsorbed APS on oxide. In view of this, other methods were explored on the basis of reducing the amount of water physisorbed onto methyl-terminated surface.

The first method involved thermal desorption at 60 °C to remove physisorbed water on methyl-terminated surfaces. The relatively low-temperature 60 °C was employed to prevent the oxide from dehydration. To explore an appropriate time for the methyl regions to be fully dehydrated, a time-series experiment (Supporting Information II) was conducted with a batch of OTS-covered samples of similar contact angle. The amount of adsorbed APS decreased linearly with heating duration and 10 hours was necessary for removal of physisorbed water, as indicated by the complete inhibition of APS deposition on OTS monolayers. Under the same conditions, a slight loss of water was also observed for hydroxyl-terminated surfaces. Figure 5b shows such a heated sample in which the attachment of Au nanoparticles has faithfully reproduced the template shown in Figure 5a. This was good evidence that the deposition of APS outside oxide domains had been completely stopped. The total efficiency of one of the domain arrays, estimated from Figure 5c, was 83%, a little lower than the value without heating as described above. Moreover, from Figure 5d it was clearly observed on ∼150-nm-diameter oxide domains only partial coverage of Au nanoparticles. The slight decrease of efficiency

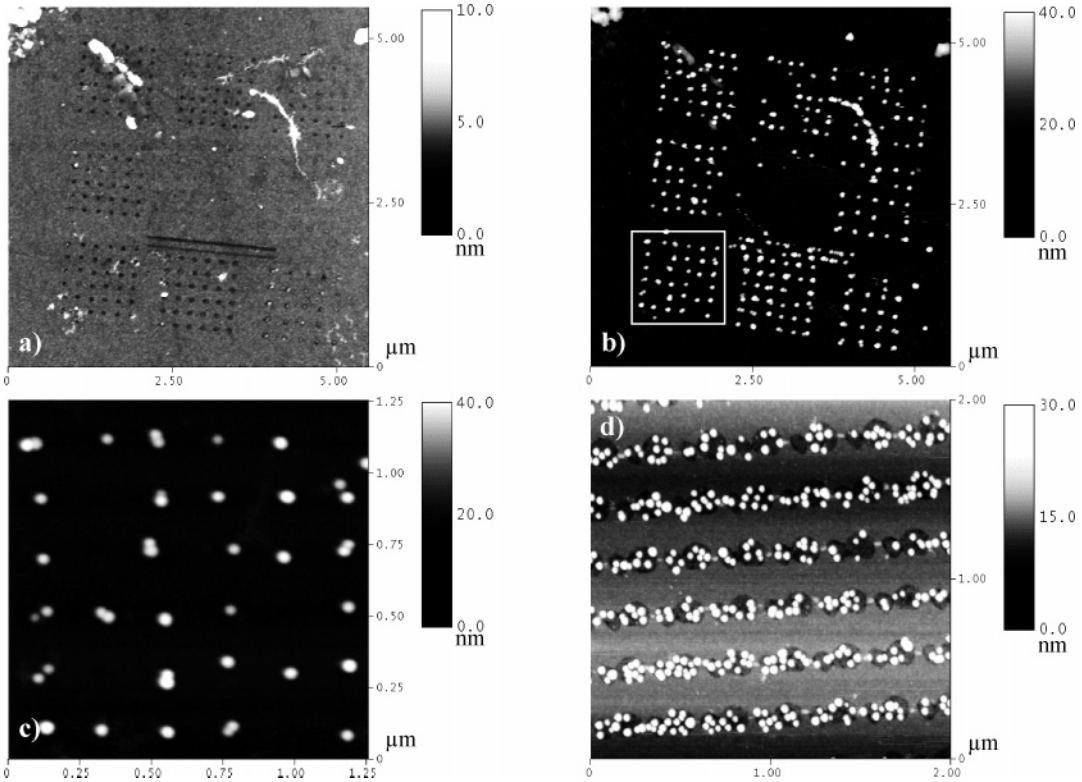

Figure 5. Tapping mode AFM topographic images of (a) an etched template of nine nanodomain arrays (6 × 6), (b) Au nanoparticles assembled onto this template that was modified with APS after the surface water outside of oxide domains was reduced by heating to 60 °C for 10 h, and (c) enlarged scan of marked square. Prepared under the same conditions, another sample with relatively large oxide domains is shown in (d).

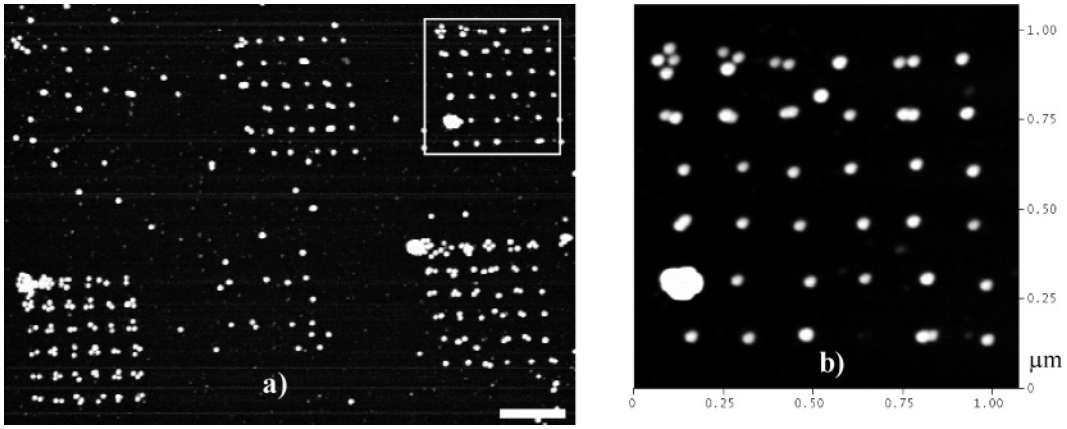

Figure 6. Tapping mode AFM topographic images of (a) Au nanoparticles assembled on an etched template composed of nanodomain arrays (6 × 6) that was modified with APS after surface water outside of oxide domains was reduced by exchanging of anhydrous solvent as described in Experimental Section and (b) enlarged scan of marked square. The extremely large dot, observed in b, could be an aggregate of Au nanoparticles already formed in their suspension. Scale bar: 500 nm. Vertical range: 30 nm.

reconfirms the important role played by water in the assembly of APS, since heating at 60 °C has no influence on hydroxyl groups on oxide.[24]

In view of this decreased efficiency and the relatively long time required to fully dehydrate samples, a further method was also examined. The details of this method were described in the Experimental Section. After etching and oxidation, the sample was rinsed sequentially with solvents of decreasing polarity. The hydrogen bonding of water with methanol would dissolve water on methyl regions into solution, and the relatively strong hydrophobic interaction between toluene and methyl moiety of OTS would favor the replacement of water on methyl regions with toluene, especially under the agitation of sonication. It is presumed that these anhydrous solvents only exchanged water physisorbed on methyl-terminated surfaces and did not affect the water hydrogen-bonded to the hydroxyl-terminated oxide domains. Without an adequate supply of surface water, APS molecules were only able to form oligomers, which could be easily removed by gentle sonication in anhydrous solvent. The best results obtained with this method are described in Figure 2 and Figure 6. From these two examples, it can be clearly identified that the physisorbed water on methyl regions was removed and only small quantities of Au nanoparticles were on these regions possibly because of the APS adsorbed at film defects. On the other hand, the water adsorbed on oxide domains was unaffected and the assembly efficiency was very high. In the 36-domain array shown in Figure 6b, only one domain was not covered with Au nanoparticles.

Such a strategy, to inhibit APS deposition outside oxide domains by reducing physisorbed water at these regions, only

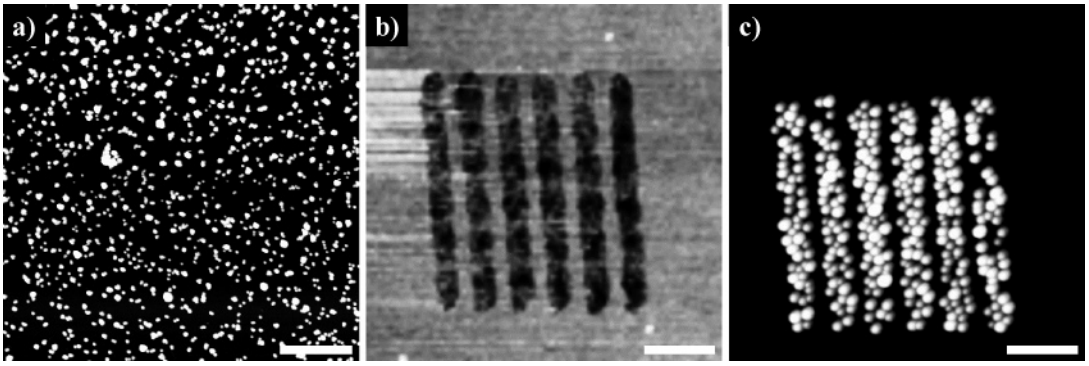

Figure 7. Tapping mode AFM topographic images of as-fabricated patterns of Au nanoparticles that were treated with wiping and readsorption cycles. One cycle for this sample: (a) methyl-terminated region before wipe, (b) patterned region immediately after wipe, (c) patterned region after the readsorption of Au nanoparticles. Scale bar: (a) 1 μm, (b) 300 nm, and (c) 300 nm. Vertical range: (a) 40 nm, (b) 10 nm, and (c) 30 nm.

produced good results on high-quality OTS monolayers, which were more resistive to the damage of etching and oxidation. For samples of relatively low-contact angles, possibly indicating the presence of unreacted Si−OH or Si−OCH_3 groups on OTS monolayers, a large number of Au nanoparticles adsorbed outside oxide domains (Figure 7a). The compact and ordered packing of OTS molecules would be disrupted by these groups, making them more susceptible to etching and acid-catalyzed hydrolysis to produce more Si−OH groups. In OTS monolayers, these reactive groups (intrinsic or developed Si−OH and Si−OCH_3 hydrolyzing into Si−OH in aqueous environments) could form covalent bonds with APS, which would be difficult to remove by sonication without damaging those adsorbed on oxide domains. Such APS molecules would determine the attachment of Au nanoparticles outside of oxide domains.

Finally, for the samples that had attracted a large number of Au nanoparticles on methyl-terminated regions, a simple method combining wiping the sample and readsorbing Au nanoparticles was effective in selectively removing those particles outside of oxide domains. For example, there were many Au nanoparticles on methyl-terminated regions (Figure 7a) before wiping; these were almost completely removed after the sample was wiped with a cotton swab (Figure 7b). Only APS deposited in the pits survived the wiping process and reattracted Au nanoparticles to its maximum (Figure 7c). Repeating the cycle several times was used to achieve the maximum effect (Supporting Information III) although some damage to the OTS monolayer was suggested by a decreasing contact angle of about 30°. With this strategy, the as-fabricated pattern could be reused to assemble Au nanoparticles of different sizes.

Conclusion

Using Au nanoparticles for APS labeling, we performed detailed investigations on the deposition of APS on silicon oxide domains produced by SPO. APS located preferentially at the domain boundaries possibly because of asymmetrically distributed hydroxyl groups, which led to the incomplete coverage of Au nanoparticles on the domains. Using oxide domains that were first etched and oxidized to cover them entirely with hydroxyl groups, greatly enhanced site-selective assembly of Au nanoparticles was consistently obtained. This ensured reproducible patterning of single Au nanoparticles when the domain size was reduced below 30 nm. Such a capability to precisely position single nano-objects onto predefined sites is crucial for the development of more complex structures. Besides the improvement brought about by hydroxyl regeneration, we also discussed the negative effect of depositing APS outside the oxide domains and described two alternative methods to overcome this. While the most promising strategy for avoidance of this unwanted deposition relies on densifying OTS monolayers and deactivating reactive groups, a simple method combining mechanical wiping and readsorbing Au nanoparticles was extremely effective. Although this work relates to specific processes for patterning Au nanoparticles, we believe the principles involved are practicable for other situations, if structures need to be developed in aqueous media or moist environments using organosilane. Investigations are ongoing to further explore the mechanism and potential of using binary monolayers of organosilane as templates to guide the assembly of nano-objects and to realize site-specific growth of nanowires using patterned Au nanoparticles as a catalyst.

Acknowledgment. This work was supported by the National Natural Science Foundation of China (NSFC 90206023), Ministry of Science and Technology of China (2001CB6105), and FOKYING TUNG Education Foundation (94012). We are grateful to Prof. C Robinson (University of LEEDS, U.K.) for his kind help and useful discussion.

Supporting Information Available: AFM height and friction images of oxide domains before and after etching, SEM evaluation for the adsorption of APS on dehydrated OTS monolayers labeled with Au nanoparticles, and additional results produced by repetition of wiping and readsorption cycles. This material is available free of charge via the Internet at http://pubs.acs.org.

References and Notes

(1) Thelander, C.; Martinsson, M. H.; Deppert, K.; Samuelson, L.; Poulsen, P. R.; Nygård, J.; Borggreen, J. *Appl. Phys. Lett.* **2001**, *79*, 2106. Ritter, C.; Heyde, M.; Schwarz, U. D.; Rademann, K. *Langmuir* **2002**, *18*, 7798. Hu, J.; Zhang, Y.; Gao, H. B.; Li, M. Q.; Hartmann, U. *Nano Lett.* **2002**, *2*, 55. Hsieh, S. C.; Meltzer, S.; Wang, C. R. C.; Requicha, A. A. G.; Thompson, M. E.; Koel, B. E. *J. Phys. Chem. B* **2002**, *106*, 231. Falvo, M. R.; Taylor, R. M., II; Helser, A.; Chi, V.; Brooks, F. P., Jr.; Washburn, S.; Superfine, R. *Nature* **1999**, *397*, 236.

(2) Cui, Y.; Björk, M. T.; Liddle, J. A.; Sönnichsen, C.; Boussert, B.; Alivisatos, A. P. *Nano Lett.* **2004**, *4*, 1093.

(3) Li, Q. G.; Zheng, J. W.; Liu, Z. F. *Langmuir* **2003**, *19*, 166.

(4) Liu, S. T.; Maoz, R.; Sagiv, J. *Nano Lett.* **2004**, *4*, 845.

(5) Liu, S. T.; Maoz, R.; Schmid, G.; Sagiv, J. *Nano Lett.* **2002**, *2*, 1055.

(6) Krämer, S.; Fuierer, R. R.; Gorman, C. B. *Chem. Rev.* **2003**, *103*, 4367.

(7) Wouters, D.; Schubert, U. S. *Angew. Chem., Int. Ed.* **2004**, *43*, 2480.

(8) Daniel, M. C.; Astruc, D. *Chem. Rev.* **2004**, *104*, 293. Shim, M.; Guyot-Sionnest, P. *Nature* **2000**, *407*, 981. Hu, J. T.; Li, L. S.; Yang, W. D.; Manna, L.; Wang, L. W.; Alivisatos, A. P. *Science* **2001**, *292*, 2060. Kong, J.; Soh, H. T.; Cassell, A. M.; Quate, C. F.; Dai, H. J. *Nature* **1998**, *395*, 878.

(9) Frens, G. *Nature Phys. Sci.* **1973**, *241*, 20.
(10) Sugimura, H.; Hozumi, A.; Kameyama, T.; Takai, O. *Surf. Interface Anal.* **2002**, *34*, 550.
(11) Zhang, F. X.; Srinivasan, M. P. *Langmuir* **2004**, *20*, 2309.
(12) Horanyi, G.; Rizmayer, E. M.; Joo, P. *J. Electroanal. Chem. Interfacial Electrochem.* **1983**, *152*, 211. Sandroff, C. J.; Herschbach, D. R. *Langmuir* **1985**, *1*, 131.
(13) Zhang, H.; He, H. X.; Wang, J.; Mu, T.; Liu, Z. F. *Appl. Phys. A* **1998**, *66*, S269.
(14) Freeman, R. G.; Grabar, K. C.; Allison, K. J.; Bright, R. M.; Davis, J. A.; Guthrie, A. P.; Hommer, M. B.; Jackson, M. A.; Smith, P. C.; Walter, D. G.; Natan, M. J. *Science* **1995**, *267*, 1629. Grabar, K. C.; Allison, K. J.; Baker, B. E.; Bright, R. M.; Brown, K. R.; Freeman, R. G.; Fox, A. P.; Keating, C. D.; Musick, M. D.; Natan, M. J. *Langmuir* **1996**, *12*, 2353. Zhu, T.; Fu, X. Y.; Mu, T.; Wang, J.; Liu, Z. F. *Langmuir* **1999**, *15*, 5197.
(15) He, H. X.; Zhang, H.; Li, Q. G.; Zhu, T.; Li, S. F. Y.; Liu, Z. F. *Langmuir* **2000**, *16*, 3846. Zheng, J. W.; Zhu, Z. H.; Chen, H. F.; Liu, Z. F. *Langmuir* **2000**, *16*, 4409.
(16) Grabar, K. C.; Smith, P. C.; Musick, M. D.; Davis, J. A.; Walter, D. G.; Jackson, M. A.; Guthrie, A. P.; Natan, M. J. *J. Am. Chem. Soc.* **1996**, *118*, 1148.
(17) Sugimura, H.; Nakagiri, N. *Langmuir* **1995**, *11*, 3623. Bloess, H.; Staikov, G.; Schultze, J. W. *Electrochim. Acta* **2001**, *47*, 335.
(18) García, R.; Calleja, M.; Pérez-Murano, F. *Appl. Phys. Lett.* **1998**, *72*, 2295. García, R.; Calleja, M.; Rohrer, H. *J. Appl. Phys.* **1999**, *86*, 1898. Moñivas, S. G.; Sáenz, J. J.; Calleja, M.; García, R. *Phys. Rev. Lett.* **2003**, *91*, 056101.
(19) Ulman, A. *Chem. Rev.* **1996**, *96*, 1533.
(20) Inoue, A.; Ishida, T.; Choi, N.; Mizutani, W.; Tokumoto, H. *Appl. Phys. Lett.* **1998**, *73*, 1976.
(21) Maoz, R.; Frydman, E.; Cohen, S. R.; Sagiv, J. *Adv. Mater.* **2000**, *12*, 725.
(22) Kurth, D. G.; Bein, T. *Langmuir* **1995**, *11*, 3061. Finklea, H. O.; Robinson, L. R.; Blackburn, A.; Richter, B.; Allara, D.; Bright, T. *Langmuir* **1986**, *2*, 239.
(23) Rye, R. R.; Nelson, G. C.; Dugger, M. T. *Langmuir* **1997**, *13*, 2965.
(24) Tripp, C. P.; Hair, M. L. *Langmuir* **1995**, *11*, 149.